



Trans. Nonferrous Met. Soc. China 34(2024) 3251-3264

Transactions of Nonferrous Metals Society of China

www.tnmsc.cn



Microstructure and properties of Cu matrix composites reinforced with surface-modified Kovar particles

Tao MENG¹, Ri-chu WANG^{1,2}, Zhi-yong CAI^{1,2}, Ying-jun YAO¹

School of Materials Science and Engineering, Central South University, Changsha 410083, China;
 Key Laboratory of Electronic Packaging and Advanced Functional Materials,
 Central South University, Changsha 410083, China

Received 30 June 2024; accepted 18 September 2024

Abstract: The thermal conductivity of Cu/Kovar composites was improved by suppressing element diffusion at the interfaces through the formation of FeWO₄ coating on the Kovar particles via vacuum deposition. Cu matrix composites reinforced with unmodified (Cu/Kovar) and modified Kovar (Cu/Kovar@) particles were prepared by hot pressing. The results demonstrate that the interfaces of Cu/FeWO₄ and FeWO₄/Kovar in the Cu/Kovar@ composites exhibit strong bonding, and no secondary phase is generated. The presence of FeWO₄ impedes interfacial diffusion within the composite, resulting in an increase in grain size and a decrease in dislocation density. After surface modification of the Kovar particle, the thermal conductivity of Cu/Kovar@ composite is increased by 110% from 40.6 to 85.6 W·m⁻¹·K⁻¹. Moreover, the thermal expansion coefficient of the Cu/Kovar@ composite is 9.8×10⁻⁶ K⁻¹, meeting the electronic packaging requirements.

Key words: electronic packaging material; Cu/Kovar composite; surface modification; thermal conductivity

1 Introduction

The coefficient of thermal expansion (CTE) of Kovar alloy closely matches that of glass, ceramic, and substrate, making it a commonly used material for hermetic packaging with glass or ceramic, as well as electronic packaging materials in tubes and integrated circuits [1–5]. However, the rapid development of the microelectronics industry has raised higher demands for both sealing materials and electronic packaging materials in terms of their thermal conductivity (TC) [6–9]. The long-term service of Kovar alloy will lead to high-temperature failure of solder joints or overheating of electronic components due to its poor TC. This results in reduced efficiency and significantly impacts the lifespan and reliability of devices. Cu, besides Au

and Ag, is a metal known for its excellent electrical and thermal conductivity [10,11]. By combining Cu with Kovar alloy into a composite, we can obtain the advantages offered by low CTE and strong weldability from Kovar alloy, while simultaneously achieving outstanding electrical and thermal conductivity from Cu. Therefore, the conflict between low CTE and high TC in Kovar alloy can be resolved through the use of Cu/Kovar composite, greatly enhancing the lifespan and reliability of highly integrated devices.

However, researchers [12,13] have shown that serious interfacial diffusion occurs during the sintering process of Fe–Co–Ni alloy powder with Cu powder. On the one hand, the entry of Ni atoms into the Cu matrix significantly reduces its TC. On the other hand, when the Ni and Co content in the alloy is less than 30%, it changes from FCC to BCC

structure, which affects the CTE of Kovar alloy. Therefore, controlling interfacial diffusion during the preparation of Kovar/Cu composites is crucial for ensuring good thermo-physical properties. Surface modification of reinforcement is an effective approach to improve the interface structure and properties. CAI et al [14] coated Si powder with a complete W coating using the sol-gel method and prepared Cu/Si composites. The results showed that W coating greatly hindered harmful interfacial reactions between Cu matrix and Si particles, reducing Cu-Si intermetallic compounds and improving the ductility of the composite. ZHANG et al [15] used the electroless plating to coat Invar alloy powder with a layer of silver before preparing the Cu/Ag(Invar) composite. The results showed that compared with non-silvercoated composite (24.1 W·m⁻¹·K⁻¹), TC was increased by 73% (41.6 W·m⁻¹·K⁻¹) in silver-coated composite. There are less published studies on the surface modification of Kovar. Therefore, surface modification of Kovar particles to improve the thermal conductivity of Cu/Kovar composites is of great significance in the field of electronic packaging.

The primary objective of this work is to employ the vacuum reaction method for coating a layer of FeWO₄ phase onto the surface of the Kovar powder particles, followed by hot pressing to prepare Cu/Kovar and coated Cu/Kovar (denoted as Cu/Kovar@) composites. Subsequently, an indepth investigation was conducted to explore the influence of the coating on the microstructure, interface behavior, and properties of these composites.

2 Experimental

The 4J29 (Fe-29%Ni-17%Co) Kovar alloy

powder, prepared by nitrogen atomization, was used with a particle size of 50–250 μm. Commercially purchased electrolytic Cu powder, with an average size of 25 μm and a range of 10–40 μm, was employed. Commercially purchased electrolytic W powder is used, with an average particle size of 0.8 μm. The morphologies of the Kovar alloy powder, Cu powder, and W powder are shown in Fig. 1. The vibrating mixer is used for powder mixing with a vibration frequency of 1200 r/min and a vibration time of 60 min. The composite consisted of Kovar powder and Cu powder in a mass ratio of 3:2. Hot pressing parameters included temperature of 800 °C, pressure of 40 MPa, and duration time of 0.5 h.

The phase analysis of the Kovar powder and Cu/Kovar composites was carried out using a Bruker D8 Focus XRD diffractometer. The microstructure of the Kovar powder and composites was observed using a JSM-7900F field emission scanning electron microscope (SEM) equipped with EDS and EBSD, as well as an F-30 transmission electron microscope (TEM). Tensile strength, yield strength, and elongation of the composites were determined using a universal mechanical testing machine. TC and CTE of the composites were measured using a laser thermal conductivity instrument and a thermal dilatometer.

3 Results and discussion

3.1 Surface modification of Kovar powder

The surface modification of the Kovar powder was carried out by mixing tungsten (W) powder with Kovar powder in different proportions, followed by vacuum deposition. Figure 2 shows the microstructures of the coating on the surface of the Kovar powder with different process parameters.

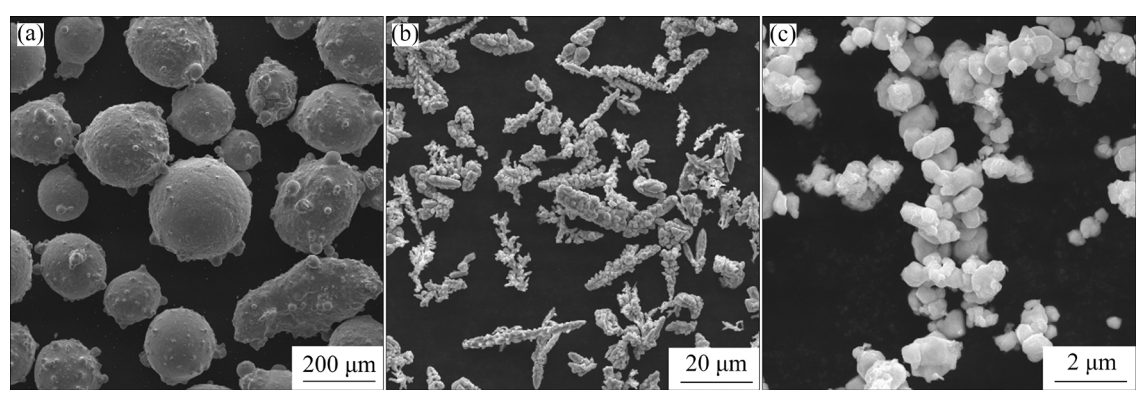


Fig. 1 Microstructure of Kovar powder (a), Cu powder (b), and W powder (c)

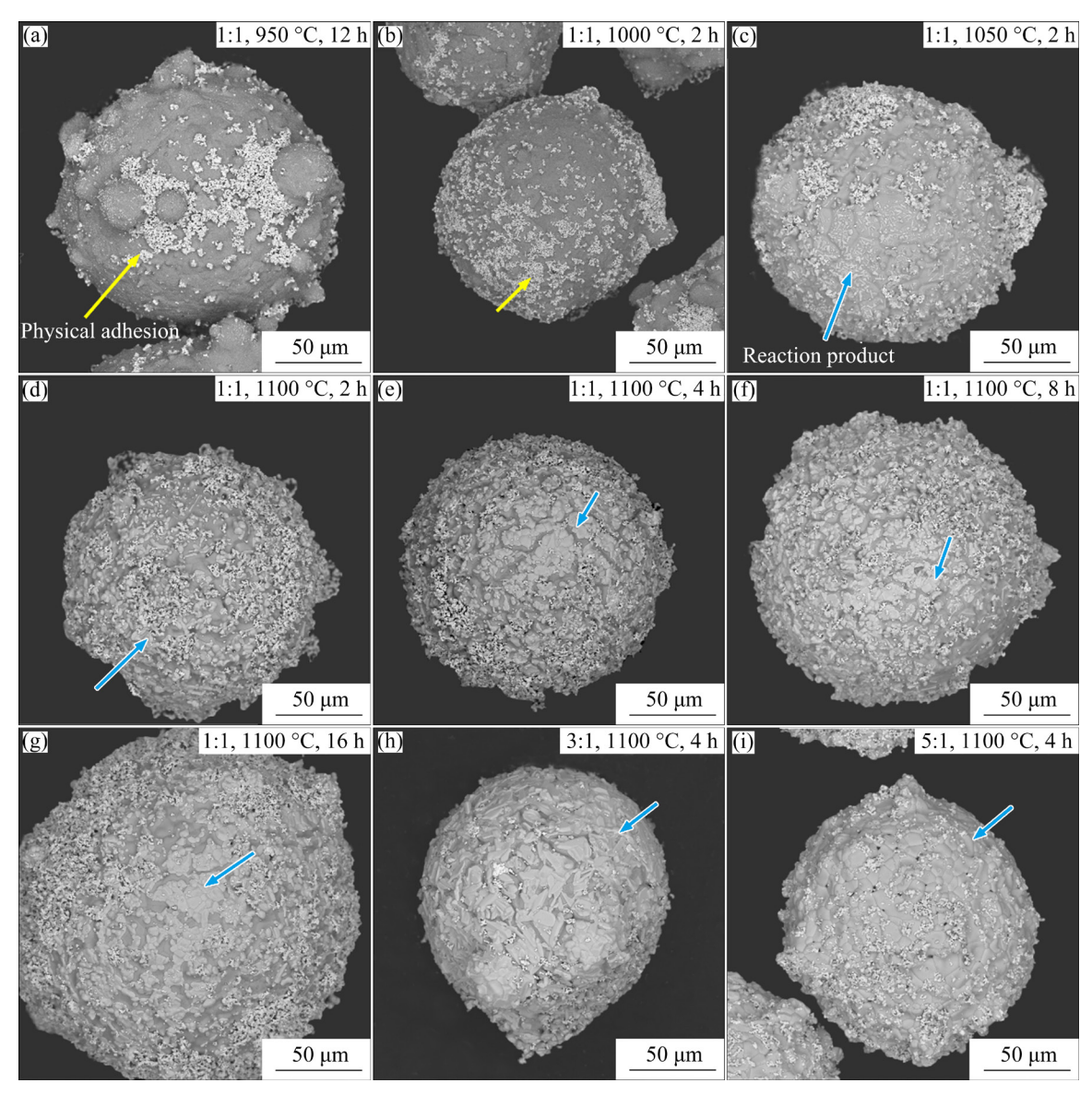


Fig. 2 Surface morphologies of Kovar particles with various process parameters of vacuum coating

Firstly, a 1:1 mass ratio mixture of Kovar and W powders was heated in a vacuum furnace at 950 °C for 2 h. Throughout the entire process, a vacuum degree ranging from 9×10⁻³ to 2×10⁻² Pa was maintained to ensure sufficient reactivity of the W powder. Under these conditions, a small amount of W powder adhered to the surface of the Kovar particles; however, complete coverage was not achieved. Keeping other parameters constant, an increase in temperature to 1000 °C resulted in partial adhesion of W powder onto the Kovar surface. At 1050 °C, new crystals began to form on the particle surfaces but were limited in number and coverage area. Further increasing the temperature to 1100 °C led to an increased number and coverage of crystals. However, increasing temperatures to above 1150 °C caused significant sintering among W powders, making it difficult to separate them from high-temperature treated mixtures with Kovar particles, and hence further experimentation could not be continued beyond this point. Therefore, a temperature of 1100 °C was selected to be optimal for conducting the coating process. The reason why W can be deposited on Kovar particles is that under high temperature and vacuum, W powder evaporates slightly and W steam is formed around Kovar particles so that W can react with Kovar particles to form deposits. Similar processes have been reported in the work of DAI et al [16].

Subsequently, an enhancement in the coating process can be pursued by altering the duration of vacuum treatment. Figures 2(e-g) show the surface

morphologies of Kovar powder treated for 4, 8, and 16 h at a temperature of 1100 °C with a mass ratio of 1:1. Upon extending the time from 2 to 4 h, there is a notable improvement observed in both the number and coverage of crystals on the surface of Kovar particles. However, further extensions to 8 and 16 h do not yield similar enhancements. This phenomenon may arise due to limitations in atom concentrations provided by an equivalent amount of W powder for facilitating surface coating reactions. Specifically, when extending the duration to 4 h, the atom concentrations supplied by W powder reach their threshold under conditions set at a ratio of 1:1, consequently leading to no additional increase in coating coverage upon further extension beyond this timeframe. Therefore, it becomes imperative to enhance the mass ratio involving W powder accordingly. Figures 2(h, i) show the coating situation on the Kovar powder surfaces when employing mass ratios of W powder to Kovar powder at 3:1 and 5:1, respectively, at a temperature of 1100 °C for 4 h. Remarkably, completely coated Kovar (Kovar@) powders are successfully obtained when utilizing a mass ratio set at 5:1.

3.2 Microstructure of Cu/Kovar composites

Figures 3 shows the XRD patterns of the Kovar powder and Cu/Kovar composites before and after coating. Prior to the coating treatment, only the face-centered cubic γ (Kovar) phase is observed in the Kovar powder. In addition to the γ phase and W phase adhering to the powder surface, there is also evidence of the FeWO₄ phase on the surface of Kovar@ powder during vacuum treatment. The reason why the diffraction peak of W is relatively high is that the target used for XRD is a Cu target. Since the ray of Cu can strongly stimulate the fluorescence of Fe elements in Kovar and FeWO₄, and the defluorination mode is used in the XRD process, the peak intensity of Kovar and FeWO₄ is very low. In fact, the content of W in Kovar@ is not high.

Combined with the microstructure of Kovar@ in Fig. 2 and XRD patterns in Fig. 3, it can be seen that W powder is partially transformed into W steam under vacuum and high temperature, and reacts with Fe element in Kovar and O element in powder to produce FeWO₄ on the surface of Kovar particles. In this process, a small part of W powder is adhered to the surface layer of FeWO₄ and a

coating layer of Kovar particles is formed together with FeWO₄.

Figure 4 shows the microstructure of the Cu/Kovar composites before and after coating. It can be seen that the Kovar particles are uniformly distributed within the Cu matrix, regardless of whether they are coated or not. Additionally, both composites exhibit dense microstructures without any noticeable voids. In Fig. 4(b), each Kovar particle is seen to be coated with FeWO₄ layer,

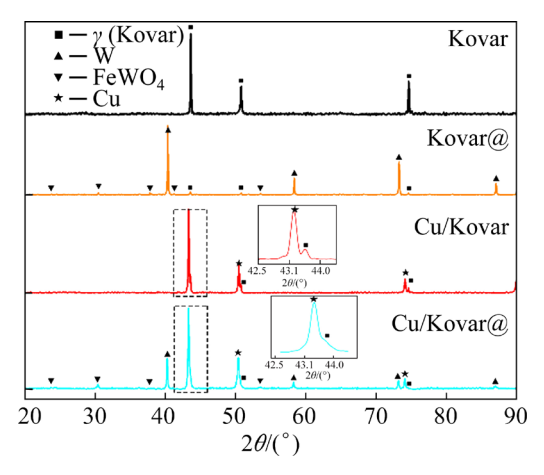


Fig. 3 XRD patterns of Kovar powders and Cu/Kovar composites

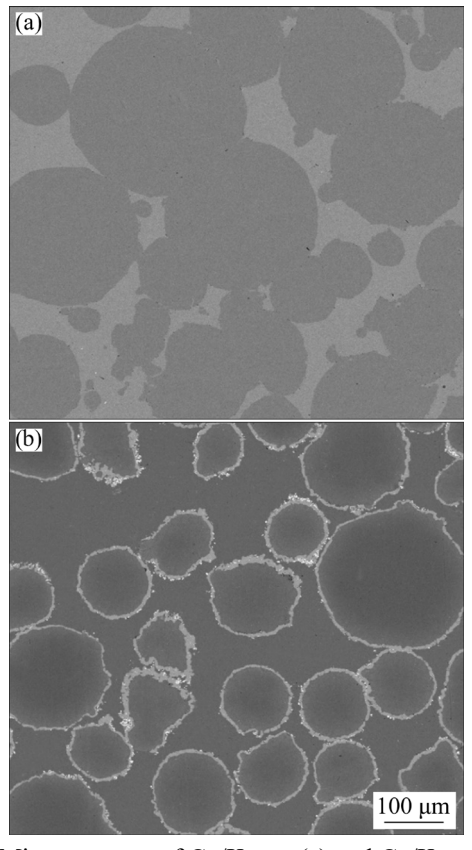


Fig. 4 Microstructure of Cu/Kovar (a) and Cu/Kovar@ (b) composite

exhibiting a coating thickness ranging from 2 to 5 μm. Moreover, there is a minor presence of adhered W particles on the surface of FeWO₄.

In order to evaluate the diffusion-inhibiting capability of the coating, the element distribution at the interface of the Cu/Kovar composite before and after coating was characterized, and the results are shown in Fig. 5. Notably, a significant exchange of elements occurs at the interface of the uncoated Kovar/Cu composites, with Fe, Co, and Ni elements present in the Cu matrix and Cu elements also found in the Kovar particles. It can be seen from Fig. 5(f) that under these sintering conditions, the mass fraction of Fe, Co, and Ni elements in the Cu matrix is 15%.

Figure 6 shows the element distribution at the interface of the Cu/Kovar@ composite. When combined with Figs. 6(b-j), it can be inferred that Fe, W, and O elements are the main components of the coating with an atomic ratio of approximately 1:1:4, indicating that FeWO₄ is present in the coating. Negligible content of Fe, Co, and Ni

elements is observed at the interface of the composite within the Cu matrix, as well as negligible content of Cu element within the Kovar particle. These observations indicate that vacuum coating plays a significant role in preventing element diffusion at the interface. Previous studies have shown that due to the structural properties of FeWO₄, a layer of chemically stable WO₃ crystals is coated on its surface, which makes the surface of FeWO₄ chemically stable [17–19]. Therefore, the FeWO₄ coating effectively inhibits element diffusion at the interface of the Cu/Kovar@ composites.

Figure 7 shows the phase distribution and grain size statistics of the Cu/Kovar and Cu/Kovar@ composites. The average grain sizes of the Cu phase and Kovar phase in the Cu/Kovar are 16.8 and 9.4 μm, respectively. In the Cu/Kovar@ composite, these values increase to 21.3 μm for the Cu phase and 14.3 μm, for the Kovar phase, respectively. The average grain size of FeWO₄ is 4.5 μm. The observed grain growth in the Kovar phase can be

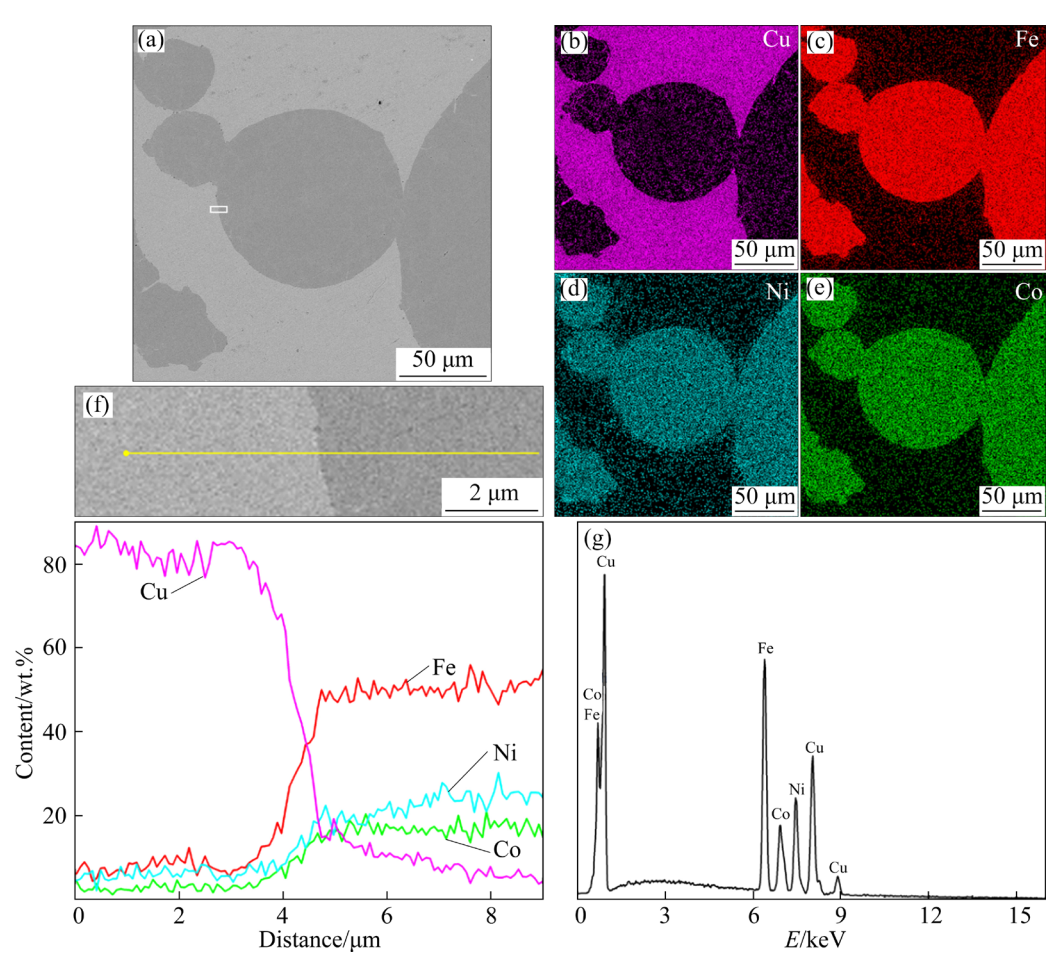


Fig. 5 Element distribution at interface of Cu/Kovar composite: (a) Microstructure; (b-e) Element mappings; (f, g) Element distribution at interface

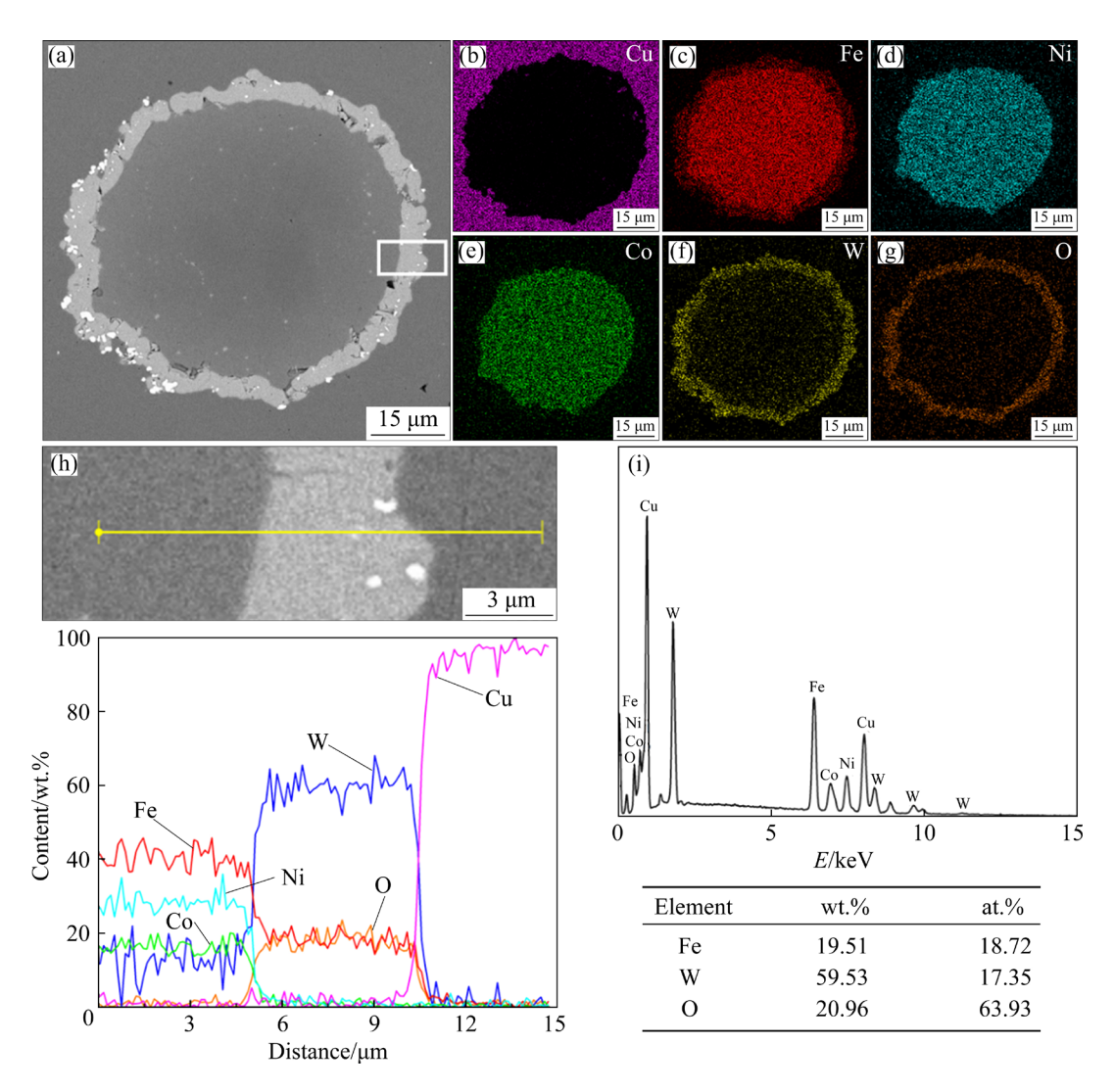


Fig. 6 Element distribution at interface of Cu/Kovar@ composite: (a) Microstructure; (b-g) Element mappings; (h, i) Element distribution at interface

attributed to recrystallization at a temperature of 900 °C [20,21], followed by subsequent grain growth during high-temperature treatment at 1100 °C for 4 h. On the other hand, changes in grain size within the Cu matrix are primarily influenced by interfacial diffusion between composite constituents during hot pressing. In the Cu/Kovar composite, diffusion of Fe, Co, and Ni elements from Kovar into the Cu matrix promotes nucleation within it, leading to refinement of grains in the Cu matrix. However, such interfacial element diffusion is significantly inhibited in the Cu/Kovar@ composite, resulting in a larger grain size of the Cu matrix.

Figure 8 shows the inverse pole figure and distribution of grain boundary misorientation angle of the Cu phase for the Cu/Kovar and Cu/Kovar@

composites. It is noteworthy that the Cu/Kovar@ composite exhibits an increased tendency in grain boundary misorientation angle compared to the Cu/Kovar composite. This result can be attributed to the merging and growth of grains, which leads to a shift from small-angle grain boundaries to large-angle grain ones. As depicted in Fig. 7, the Cu phase in the Cu/Kovar@ composite possesses a larger grain size than that in the Cu/Kovar composite. Consequently, Kovar particles with coating result in an increase in misorientation angle at the grain boundaries of the composite. Furthermore, it is believed that small-angle grain boundaries are formed through dislocation recombination [22]. Therefore, the transformation from small angles to large angles also indicates a reduction in dislocation density within the Cu matrix.

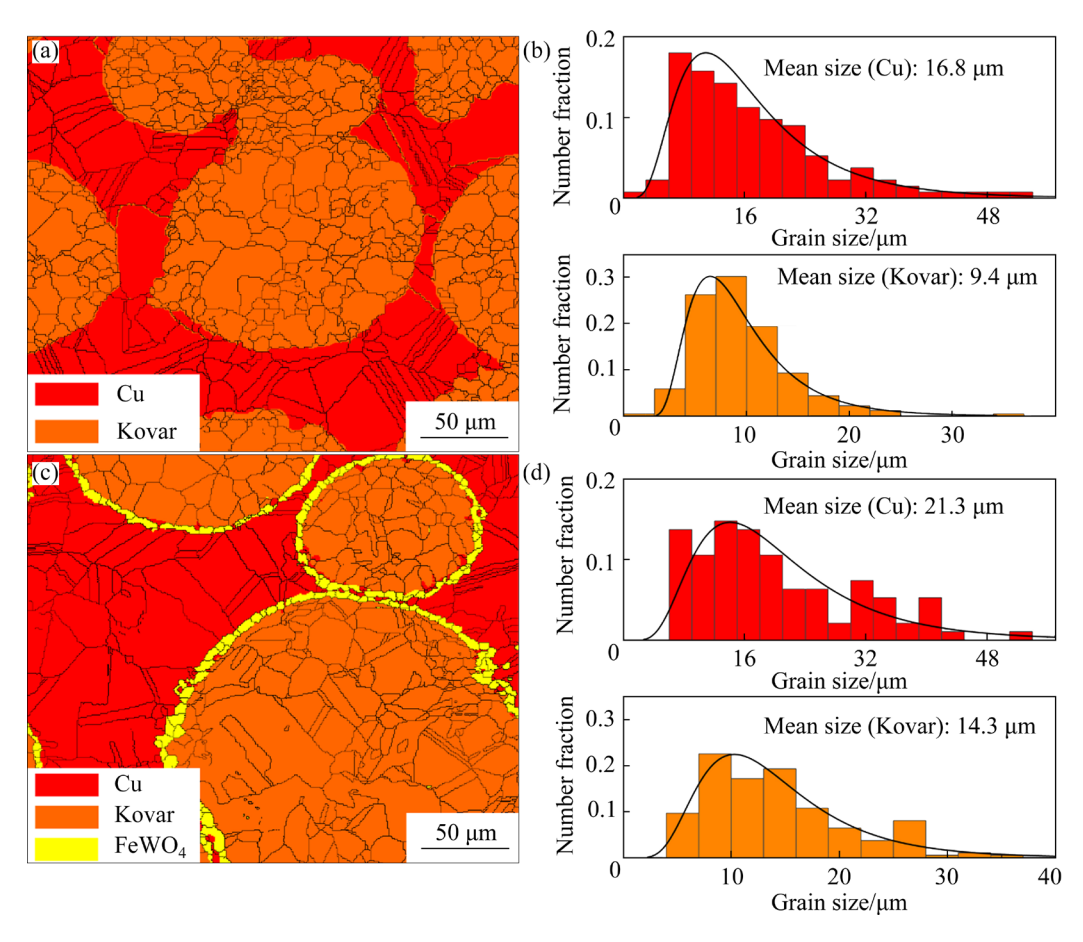


Fig. 7 Phase distribution (a, c) and grain size (b, d) of Cu/Kovar (a, b) and Cu/Kovar@ (c, d) composites

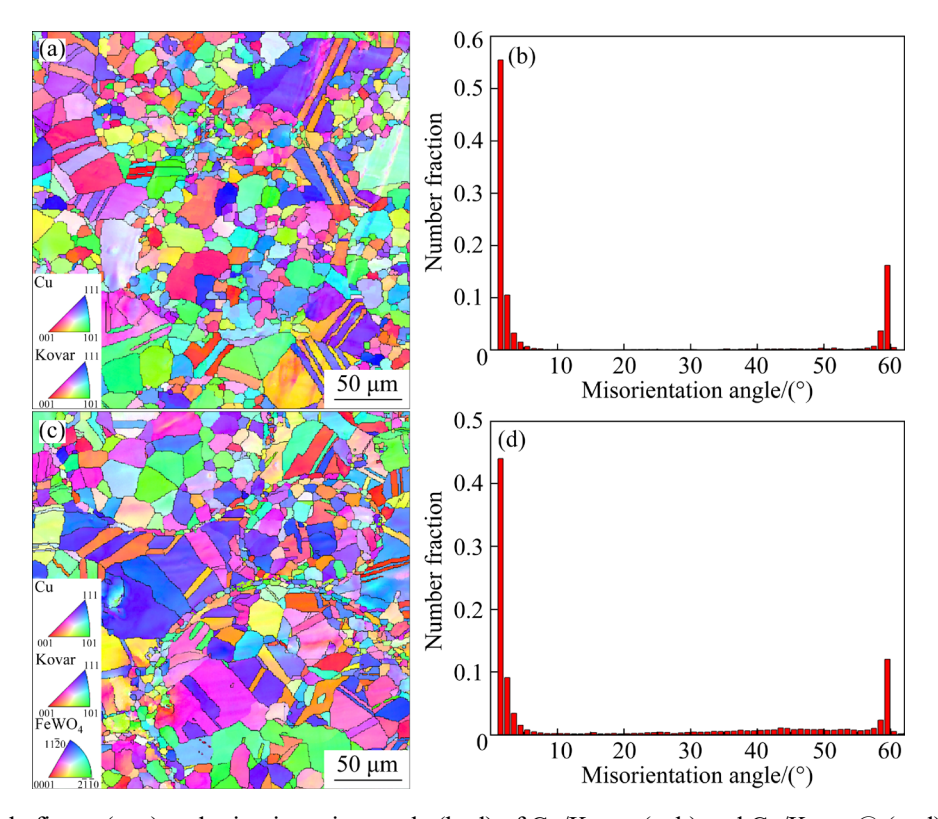


Fig. 8 Inverse pole figure (a, c) and misorientation angle (b, d) of Cu/Kovar (a, b) and Cu/Kovar@ (c, d) composites

Figure 9 shows kernel average misorientation (KAM) maps of Cu/Kovar and Cu/Kovar@ composites. The value of KAM can reflect the local strain. It can be seen that there is a certain local strain at the interface of Cu/Kovar composites after sintering due to the large difference in the coefficient of thermal expansion between the Cu phase and Kovar phase. In the Cu/Kovar@ composite, the local strain is mainly concentrated in the FeWO4 layer, which reduces the local strain in the Cu phase and Kovar phase. This is because FeWO4 acts as a transition layer between Cu and Kovar, alleviating the interaction between Cu and

Kovar phases.

Figure 10 shows the microstructure at the interface of the Cu/Kovar composite. Despite significant element diffusion, no second phase formation occurs at the interface, which aligns with the observations from XRD results shown in Fig. 3. Specifically, the angles between the Cu phase and Kovar compact plane and the interface are 41° and 2°, respectively. The lattice mismatch (δ) between the two phases can be calculated using the following formula [23,24]:

$$\delta = |a_1 - a_2|/a_1 \tag{1}$$

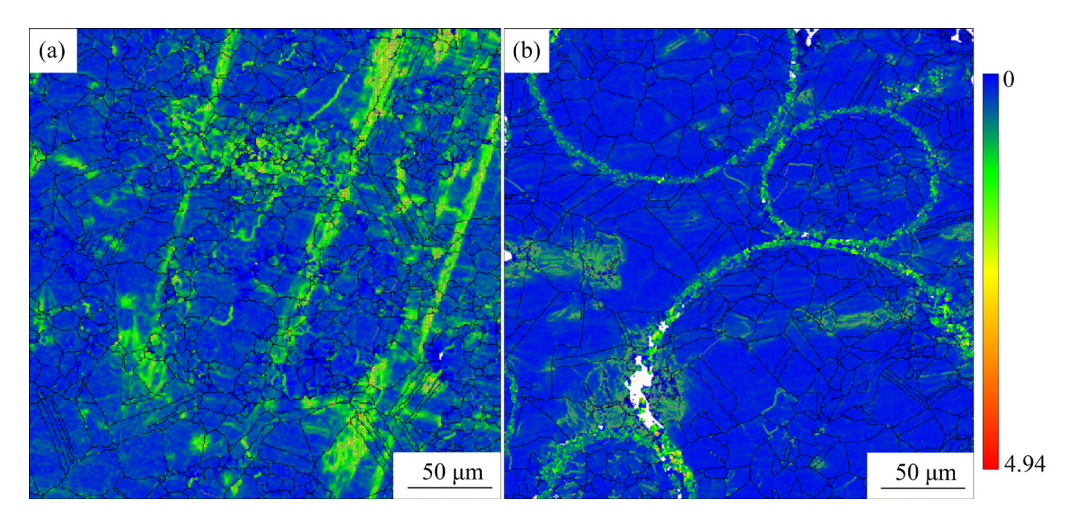


Fig. 9 KAM maps of Cu/Kovar (a) and Cu/Kovar@ (b) composite

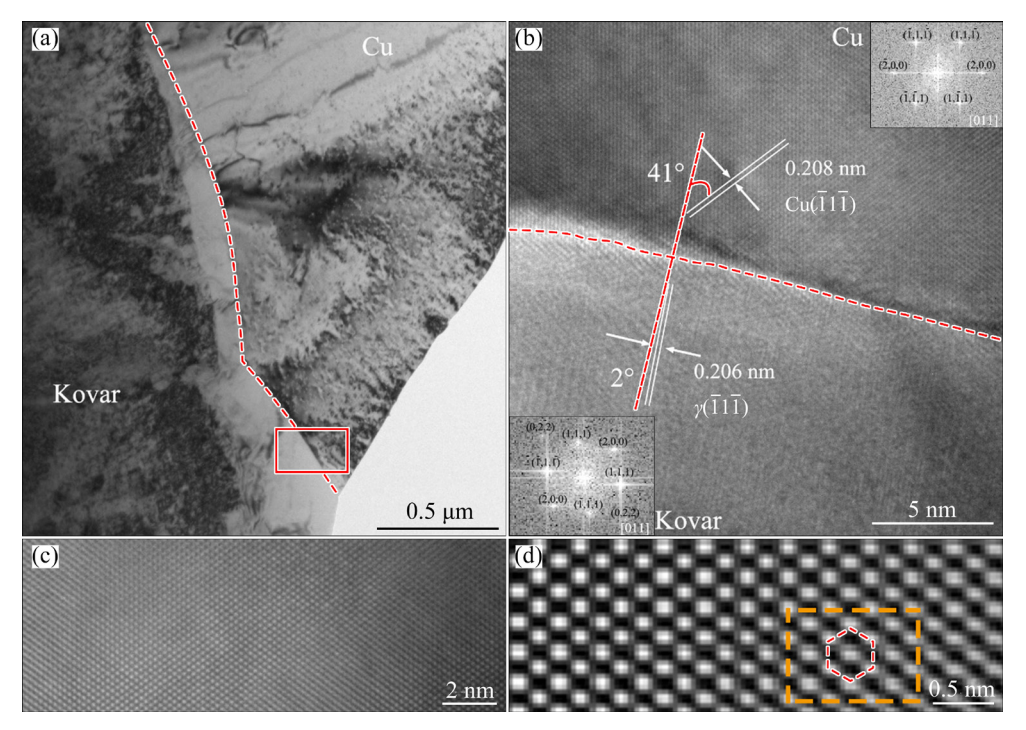


Fig. 10 Interfacial microstructures of Cu/Kovar composite (a, b); HRTEM (c) and IFFT (d) of Cu phase (The red dashed lines depict the ideal lattice position)

where a is the crystal plane spacing. The calculated $\delta_{\text{(Cu-Kovar)}}$ is 25.21%, indicating a non-coherent interface between Cu and Kovar. Figures 10(c, d) depict a high-resolution TEM (HRTEM) structure and inverse fast Fourier transform (IFFT) image of the Cu phase. It can be observed that the Cu phase exhibits slight lattice distortion due to the diffusion of Fe, Co, and Ni atoms.

Figure 11 shows the microstructure at the interface of the Cu/Kovar@ composite. The composition of the coating, FeWO₄, is further confirmed by the fast Fourier transform shown in Fig. 11(e). As observed from Figs. 11(a–f), both the interfaces of Cu phase and FeWO₄ (Cu/FeWO₄) and FeWO₄ phase and the Kovar phase (FeWO₄/Kovar) exhibit excellent combination without any

generation of second phases. The angles between the Cu phase and FeWO₄ phase as well as their respective interface are measured to be 27° and 57°, while those between the FeWO₄ phase and Kovar phase along with their corresponding interfaces are found to be 31° and 53°, respectively. The $\delta_{\text{(Cu/FeWO_4)}}$ and $\delta_{\text{(FeWO_A/Kovar)}}$ values of 51.66% and 10.36%, indicate non-coherent and semi-coherent interfaces, respectively. The non-coherence at the interface between FeWO₄ and Cu phase can be attributed to the randomness during hot pressing for forming an interface between them. On the other hand, a semi-coherent interface is formed between FeWO₄ and Kovar due to its in-situ generation on the Kovar phase, where low energy facilitates the growth of FeWO₄ crystals through coherent or semi-coherent

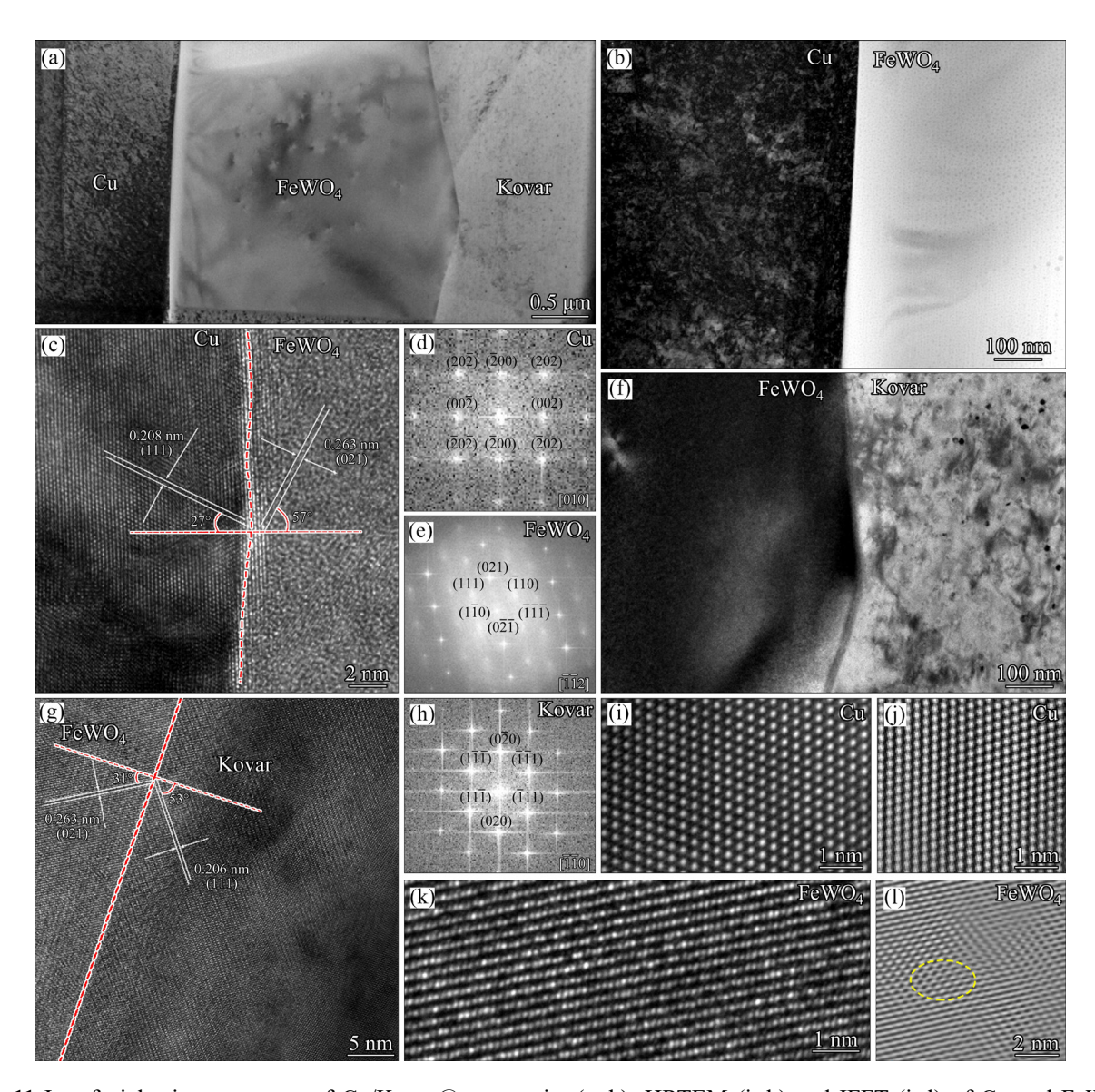


Fig. 11 Interfacial microstructures of Cu/Kovar@ composite (a-h); HRTEM (i, k) and IFFT (j, l) of Cu and FeWO₄ phase

interactions at this interface. Moreover, it should be noted that compared to non-coherent interfaces, the semi-coherent interface formed by FeWO₄–Kovar exhibits superior heat transfer efficiency.

3.3 Properties of Cu/Kovar composites

The mechanical properties of the Cu/Kovar and Cu/Kovar@ composites are presented in Fig. 12. Compared with the Cu/Kovar composite, the ultimate tensile strength and yield strength of the Cu/Kovar@ composite decrease from 385 and 250 MPa to 360 and 224 MPa, respectively, while the elongation decreases from 14.3% to 10.4%. On the one hand, the diffusion is inhibited leading to weakened solid solution strengthening in the Cu matrix. On the other hand, the increased grain size and decreased dislocation density contribute to a decrease in strength. The reduction in elongation is primarily attributed to the grain growth.

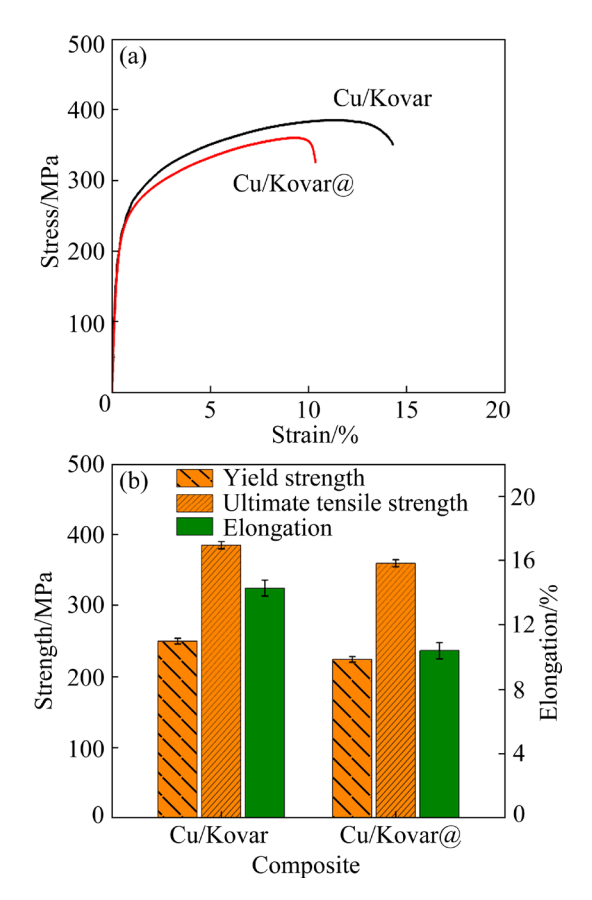


Fig. 12 Tensile stress-strain curves (a) and mechanical properties (b) of Cu/Kovar and Cu/Kovar@ composites

The thermo-physical properties of the Cu/Kovar and Cu/Kovar@ composites are presented in Fig. 13. Compared with the Cu/Kovar composite, the TC and CTE of the Cu/Kovar@

composite change from 40.6 W·m⁻¹·K⁻¹ and 9.1×10⁻⁶ K⁻¹ to 85.4 W·m⁻¹·K⁻¹ and 9.8×10⁻⁶ K⁻¹, respectively, representing an increase of TC by 110.3% and CTE by 7.7%. The presence of Fe, Co, and Ni atoms can reduce the thermal expansion coefficient of the Cu matrix [12,25]. Therefore, the observed increase in CTE is due to inhibited interfacial diffusion and reduced solute atoms within the Cu matrix.

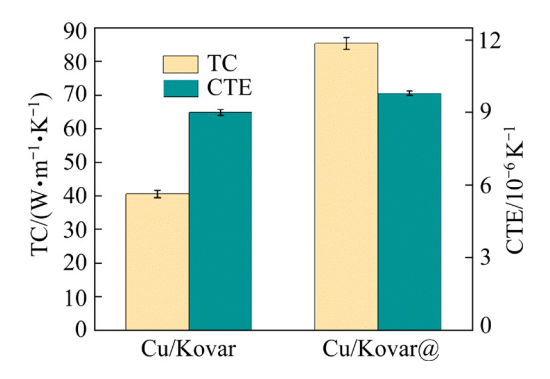


Fig. 13 Thermo-physical properties of Cu/Kovar and Cu/Kovar@ composites

The TC of composites reinforced with spherical particles can be predicted using Hasselman–Johnson theoretical model [26], which takes into account the impact of particle size, volume fraction, and interface thermal resistance on the TC of these composites:

$$k = k_{\rm m} \frac{2(k_{\rm p}/k_{\rm m} - k_{\rm p}/h_{\rm c}r - 1)v_{\rm f} + k_{\rm p}/k_{\rm m} + 2k_{\rm p}/h_{\rm c}r + 2}{(1 - k_{\rm p}/k_{\rm m} + k_{\rm p}/h_{\rm c}r)v_{\rm f} + k_{\rm p}/k_{\rm m} + 2k_{\rm p}/h_{\rm c}r + 2}$$
(2)

where k is the TC of composite, k_p is the TC of particles, k_m is the TC of matrix, v_f is the volume fraction of particles, h_c is the interfacial thermal conductance, and r is the radius of particles.

The interface thermal conductivity can be estimated by Eqs. (3) and (4) [27]:

$$h_{\rm c} \approx \frac{1}{2} \rho_{\rm m} C_{\rm m} \frac{v_{\rm m}^3}{v_{\rm p}^2} \frac{\rho_{\rm m} \rho_{\rm p} v_{\rm m} v_{\rm p}}{\left(\rho_{\rm m} v_{\rm m} + \rho_{\rm p} v_{\rm p}\right)^2}$$
 (3)

$$v = \sqrt{E/\rho} \tag{4}$$

where ρ is the density, C is the specific heat capacity, v is the phonon Debye velocity, and E is the elastic modulus. The parameters utilized for the calculation of the theoretical TC are listed in Table 1.

Table 1 Parameters for calculating theoretical TC of Cu/Kovar@ composite

Phase	Density/ (g·cm ⁻³)	Specific heat capacity/ (J·kg ⁻¹ ·K ⁻¹)	Elastic modulus/ GPa	$TC/ (W \cdot m^{-1} \cdot K^{-1})$
Cu	8.9	390	127	385
FeWO ₄	7.5	34	143	2
Kovar	8.2	650	138	17

The interfacial thermal conductance between Kovar and FeWO₄ is $h_{c1}=2.41\times10^9\,\mathrm{W\cdot m^{-2}\cdot K^{-1}}$, that between FeWO₄ and Cu is $h_{c2}=1.23\times10^9\,\mathrm{W\cdot m^{-2}\cdot K^{-1}}$, and that between Kovar and Cu is $h_{c3}=1.39\times$ 10⁹ W⋅m⁻²⋅K⁻¹. The calculated theoretical TC values of the Cu/Kovar and Cu/Kovar@ composites are 131.9 and 125.6 W·m⁻¹·K⁻¹, respectively. The deviation of the experimental thermal conductivity of Cu/Kovar is 224.8% compared with the theoretical value. Obviously, this is due to the decrease of thermal conductivity caused by the diffusion of Fe, Co and Ni elements in Kovar particles into the Cu matrix. The thermal conductivity of Cu/Kovar@ is increased by 110.3% compared with Cu/Kovar. This significant enhancement in TC can be attributed to the effective inhibition of element diffusion at the composite interface, as well as varying degrees of grain size enlargement in both the Cu phase and Kovar phase along with a decrease in dislocation density within the Cu phase, which promotes heat transfer within the composites.

The theoretical thermal conductivity of Cu/Kovar is lower than that of Cu, due to the lower thermal conductivity of FeWO₄ than that of Kovar. However, there exists a discrepancy between the actual value and the theoretical value of TC of Cu/Kovar@ composite due to lattice mismatch at the interface of the Cu phase and FeWO₄ phase. As shown in Figs. 11(i–l), minimal lattice distortion can be observed in the Cu phase, whereas significant lattice distortion occurs in the FeWO₄ phase.

characterize accurately this distortion in FeWO₄, local strain components of Cu/Kovar@ composite were analyzed using the geometric phase (GP) method [28,29], and the results are shown in Fig. 14. The lattice strain values are higher in the FeWO₄ phase compared to those in both Cu and Kovar phases, indicating severe lattice distortion within the FeWO₄ phase. Figure 15 illustrates the image quality (IQ) maps of the Cu/Kovar composite. Previous studies [30,31] have demonstrated that the IQ maps can reflect the lattice distortion with a lower image quality value corresponding to greater lattice distortion. The FeWO₄ coating exhibits relatively serious lattice distortion, which is consistent with the results in Fig. 11(1) and Fig. 14. This may be attributed to significant differences in CTE between Cu and Kovar, resulting in substantial lattice distortion of FeWO₄ during hot pressing and cooling processes. These factors contribute to the deviation between the actual TC values and the theoretical predictions.

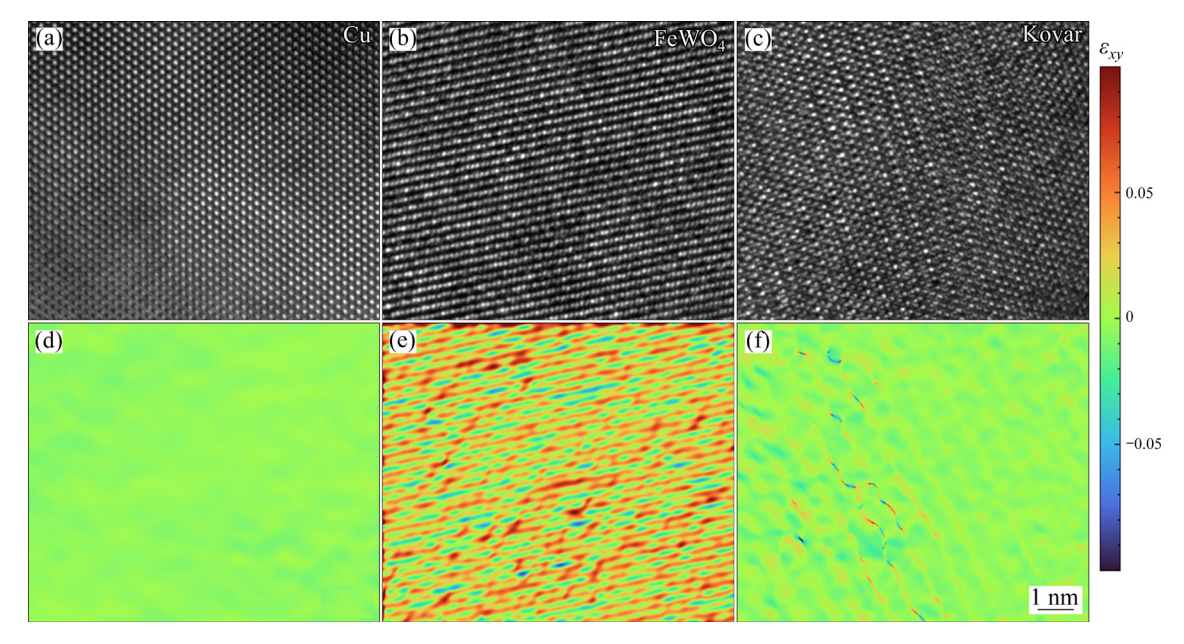


Fig. 14 Lattice distortion (ε_{xy}) distribution of Cu/Kovar@ composite

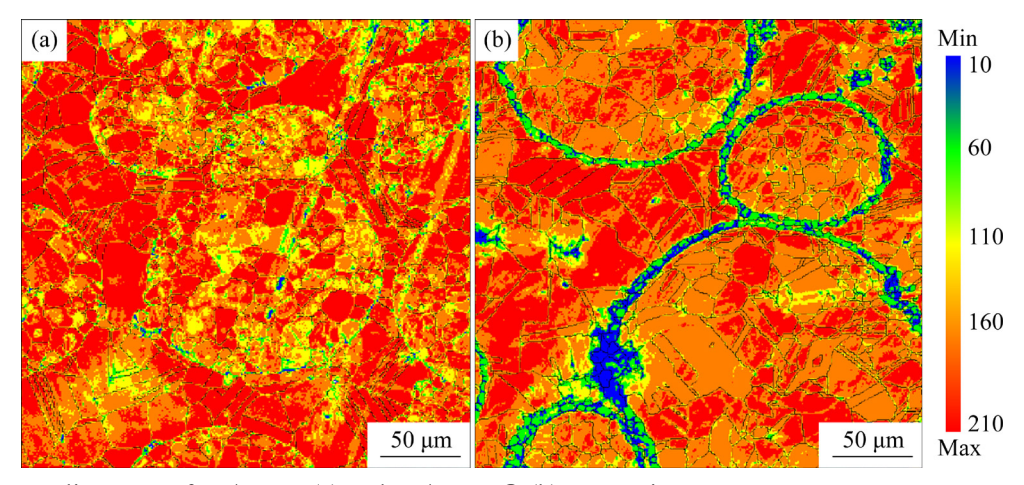


Fig. 15 Image quality maps of Cu/Kovar (a) and Cu/Kovar@ (b) composites

4 Conclusions

- (1) The surface of Kovar particles is successfully coated with a layer of FeWO₄ through vacuum deposition. A complete coating is achieved after subjecting the mixture of W and Kovar powder to the treatment at 1100 °C for 4 h, with a mass ratio of 5:1. The FeWO₄ coating effectively hinders the interfacial element diffusion in the Cu/Kovar@ composite.
- (2) Compared with the Cu/Kovar composite, the grain size of the Cu/Kovar@ composite increases and the solid solution strengthening decreases due to the inhibition of interfacial diffusion. So, the ultimate tensile strength and yield strength of Cu/Kovar composite decrease from 385 and 250 MPa to 360 and 224 MPa, respectively, and the elongation decreases from 14.3% to 10.4%.
- (3) Due to the effective inhibition of interfacial element diffusion by FeWO₄ coating, the TC of the Cu/Kovar@ composite is significantly enhanced from 40.6 to 85.4 W·m⁻¹·K⁻¹, representing a remarkable increase of 110.3%, while the CTE is only increased by 7.7% when compared with the Cu/Kovar composite.

CRediT authorship contribution statement

Tao MENG: Conceptualization, Methodology, Writing – Original draft preparation; **Ri-chu WANG:** Writing – Reviewing and editing, Supervision; **Zhi-yong CAI:** Writing – Reviewing and editing; **Ying-jun YAO:** Data curation, Formal analysis.

Declaration of competing interest

The authors declare that they have no known

competing financial interests or personal relationships that could have appeared to influence the work reported in this paper.

Acknowledgments

The authors are grateful for the financial support provided by the National Natural Science Foundation of China (No. 52274369), and the Science and Technology Program of Hunan Province, China (No. 2020GK2044).

References

- RYELANDT S, MERTENS S, DELANNAY F. Al/stainlessinvar composites with tailored anisotropy for thermal management in light weight electronic packaging [J]. Materials & Design, 2015, 85: 318-323.
- [2] CHEN Guo-qing, YIN Qian-xing, DONG Zhi-bo, ZHANG Ge, LI Yu-long, ZHAO Yu-xing, ZHANG Bing-gang, HUANG Yong-xian. Microstructure evolution analysis for the reaction interface between molybdenum and Kovar acquired by electron beam welding-brazing [J]. Materials Characterization, 2021, 171: 110781.
- [3] LU Jin-xia, GAN Xue-ping, LIU Chao-qiang. Microstructures and properties of Cu/Fe/Kovar composites prepared with Cu-coated Kovar alloy powders [J]. Materials Letters, 2024, 362: 136218.
- [4] XIN Cheng-lai, LIU Wen-bo, LI Ning, YAN Jia-zhen, SHI San-qiang. Metallization of Al₂O₃ ceramic by magnetron sputtering Ti/Mo bilayer thin films for robust brazing to Kovar alloy [J]. Ceramics International, 2016, 42: 9599–9604.
- [5] WU Hao-yue, LI Xue-wen, TU Bing, ZHANG Lin, PAN Pan, LI Yu-long. Microstructure and mechanical properties of single-crystal diamond/Kovar alloy joints brazed with an AgCuTi metal filler [J]. Diamond and Related Materials, 2023, 138: 110246.
- [6] LI Rui-yi, YANG Xiao, LI Jian, SHEN Ya-nan, ZHANG Li-xin, LU Rui, WANG Chun, ZHENG Xing-hua, CHEN Hai-sheng, ZHANG Ting. Review on polymer composites with high thermal conductivity and low dielectric properties for electronic packaging [J]. Materials Today Physics, 2022,

- 22: 100594.
- [7] ZHOU Wei, WANG Ri-chu, PENG Chao-qun, CAI Zhi-yong. Microstructure and properties of Al-Si/Al-SiC_p bilayer composite for electronic packaging [J]. Journal of Materials Science-Materials in Electronics, 2022, 33(10): 7811-7823.
- [8] ZHANG Yue-hua, HAO Ning-ke, LIN Xue-jiao, NIE Shuang-xi. Emerging challenges in the thermal management of cellulose nanofibril-based supercapacitors, lithium-ion batteries and solar cells: A review [J]. Carbohydrate Polymers, 2020, 234: 115888.
- [9] ZHOU Wei, WANG Ri-chu, PENG Chao-qun, CAI Zhi-yong. Microstructure and properties of Al–Si functionally graded materials for electronic packaging [J]. Transactions of Nonferrous Metals Society of China, 2023, 33: 3583–3596.
- [10] LI Xian-long, GUO Bai-song, YU Xiang, YANG Chuang-chuang, ZHOU Sheng-feng, CUI Shao-gang, ZHANG Zhi-guo, LI Wei. Particle morphology dependence of the mechanical and electrical properties in the in-situ graphene reinforced Cu matrix composites [J]. Composites Part A: Applied Science and Manufacturing, 2024, 179: 108032.
- [11] XIE Zhong-nan, GUO Hong, XIAO Wei, ZHANG Xi-ming, HUANG Shu-hui, SUN Ming-mei, XIE Hao-feng. Interfacial structures and their effect on thermal conductivity and mechanical properties of diamond/Cu-B composites [J]. Transactions of Nonferrous Metals Society of China, 2024, 34: 246-254.
- [12] GAO Ling, MENG Tao, XU Guo-fu, WANG Ri-chu, PENG Chao-qun, CAI Zhi-yong. Interfacial diffusion behavior and properties of hot-pressed Kovar/Cu composites [J]. Materials Chemistry and Physics, 2024, 315: 128957.
- [13] WU Dan, WU Shi-Pu, YANG Lei, TANG Wen-ming. Preparation of Cu/Invar composites by powder metallurgy [J]. Powder Metallurgy, 2015, 58: 100–105.
- [14] CAI Zhi-yong, WEN Jing, WANG Ri-chu, PENG Chao-qun, LI Xin-xing, LI Zi-ming, KANG Zhi-jie. Characteristics of tungsten coating on silicon particles prepared by sol-gel method [J]. Materials Chemistry and Physics, 2023, 305: 127942.
- [15] ZHANG Xin, WU Dn, YANG Lei, SHI Chang-dong, WU Yu-cheng, TANG Wen-ming. Microstructures and properties of Cu/Ag(Invar) composites fabricated by powder metallurgy [J]. Transactions of Nonferrous Metals Society of China, 2017, 27: 1759–1766.
- [16] DAI Shu-gang, LI Jin-wang, WANG Chang-ji. Preparation and thermal conductivity of tungsten coated diamond/copper composites [J]. Transactions of Nonferrous Metals Society of China, 2022, 32: 2979–2992.
- [17] LI Jian-hua, XIE Jia-hao, WANG Xin-yu, DAI Ying, XU Xiao-qin, LIU Jin, CAI Zhuang, MENG Xin, ZOU Jin-long. Acid-stable CoWO₄/WO₃-microrod coated by a thin carbon-layer as efficient Pt Co-catalysts for methanol oxidation and oxygen reduction [J]. Chinese Journal of Structural Chemistry, 2022, 41: 2207059–2207067.
- [18] WU Jian-chun, SHEN Xi-cheng, WANG Huan, DENG Dai-jie, WU Su-qin, GONG Yue, ZHU Lin-hua, XU Li, LI He-nan. Electronic structure modification of FeWO₄ through F doping for enhanced oxygen reduction performance in zinc-air batteries [J]. Materials Today Physics, 2023, 38: 101274.
- [19] SHI Xiao-qiang, WANG Li-na, ZUH A A, JIA Yue-fa, DING

- Fei, CHENG Hong-fei, WANG Qi-zhao. Photo-fenton reaction for the degradation of tetracycline hydrochloride using a FeWO₄/BiOCl nanocomposite [J]. Journal of Alloys and Compounds, 2022, 903: 163889.
- [20] YAZDANI M, ABBASI S M, TAHERI A K, MOMENI A, Hot deformation behavior of Fe-29Ni-17Co alloy [J]. Transactions of Nonferrous Metals Society of China, 2013, 23: 3271-3279.
- [21] YAZDANI M, ABBASI S M, MOMENI A, TAHERI A K, Design. Hot ductility of a Fe-Ni-Co alloy in cast and wrought conditions [J]. Materials & Design, 2011, 32: 2956-2962.
- [22] MENG Tao, FENG Yan, PENG Chao-qun, CAI Zhi-yong, WANG Meng. Microstructure, mechanical and thermophysical properties of hot-rolled Mo-50Cu composite [J]. Journal of Alloys and Compounds, 2023, 942: 168997.
- [23] BAI Guang-zhu, WANG Lu-hua, ZHANG Yong-jian, WANG Xi-tao, WANG Jin-guo, KIM M J, ZHANG Hai-long. Tailoring interface structure and enhancing thermal conductivity of Cu/diamond composites by alloying boron to the Cu matrix [J]. Materials Characterization, 2019, 152: 265–275.
- [24] LI Shi-cheng, LIANG Hong-yan, LI Chong, LIU Yongchang. Lattice mismatch in Ni₃Al-based alloy for efficient oxygen evolution [J]. Journal of Materials Science & Technology, 2022, 102: 19–27.
- [25] BAI Guang-zhu, WANG Lu-hua, ZHANG Yong-jian, WANG Xi-tao, WANG Jin-guo, KIM M J, ZHANG Hai-long. Tunable coefficient of thermal expansion of Cu-B/diamond composites prepared by gas pressure infiltration [J]. Journal of Alloys and Compounds, 2019, 794: 473–481.
- [26] DAI Shu-gang, LI Jin-wang, LU Ning-xiang, Research progress of diamond/copper composites with high thermal conductivity [J]. Diamond and Related Materials, 2020, 108: 107993.
- [27] ZHU Ping, ZHANG Qiang, QU Shuo, WANG Zhi-jun, GUO Hua-song, SHILKO S V, KOBAYASHI E, WU Gao-hui. Effect of interface structure on thermal conductivity and stability of diamond/aluminum composites [J]. Composites Part A: Applied Science and Manufacturing, 2022, 162: 107161.
- [28] HŸTCH M J, SNOECK E, KILAAS R. Quantitative measurement of displacement and strain fields from HREM micrographs [J]. Ultramicroscopy, 1998, 74: 131–146.
- [29] HŸTCH M J, PUTAUX J L, PÉNISSON J M. Measurement of the displacement field of dislocations to 0.03 Å by electron microscopy [J]. Nature, 2003, 423: 270–273.
- [30] RUI Shao-shi, HAN Qi-nan, WANG Xue, LI Shan-lin, MA Xian-feng, SU Yue, CAI Zhi-peng, DU Dong, SHI Hui-ji. Correlations between two EBSD-based metrics kernel average misorientation and image quality on indicating dislocations of near-failure low alloy steels induced by tensile and cyclic deformations [J]. Materials Today Communications, 2021, 27: 102445.
- [31] ZHANG Yong-jian, BAI Guang-zhu, ZHU Xiang-yu, DAI Jing-jie, WANG Xi-tao, WANG Jin-guo, KIM M J, ZHANG Hai-long. Manipulating in-situ discrete carbide interlayer to achieve high thermal conductivity in Cu–B/diamond composite [J]. Materials Today Communications, 2023, 34: 105357.

表面改性 Kovar 颗粒增强 Cu 基复合材料的显微组织与性能

孟涛1, 王日初1,2, 蔡志勇1,2, 姚映君1

- 1. 中南大学 材料科学与工程学院,长沙 410083;
- 2. 中南大学 电子封装与先进功能材料重点实验室,长沙 410083

摘 要:通过真空沉积在 Kovar 颗粒上形成 FeWO₄涂层,抑制元素在界面处的扩散,从而提高 Cu/Kovar 复合材料的热导率。采用热压法制备了未改性(Cu/Kovar)和改性 Kovar 颗粒增强(Cu/Kovar@)的 Cu 基复合材料。结果表明:Cu/Kovar@复合材料中 Cu/FeWO₄和 FeWO₄/Kovar 界面结合较强,且未产生二次相;FeWO₄的存在阻碍了复合材料内部界面的扩散,导致晶粒尺寸增大和位错密度降低。Kovar 颗粒进行表面改性后,Cu/Kovar@复合材料的热导率从 $40.6~\mathrm{W\cdot m^{-1}\cdot K^{-1}}$ 提高到 $85.6~\mathrm{W\cdot m^{-1}\cdot K^{-1}}$,提高了 110%。Cu/Kovar@复合材料的热膨胀系数为 $9.8\times10^{-6}~\mathrm{K^{-1}}$,可满足电子封装要求。

关键词: 电子封装材料; Cu/Kovar 复合材料; 表面改性; 热导率

(Edited by Bing YANG)